Photocrosslinkable and Elastomeric Hydrogels for Bone Regeneration

Teena Thakur[1], Janet R. Xavier[1], Lauren Cross[1], Manish K. Jaiswal[1], Eli Mondragon[1], Roland Kaunas[1,], Akhilesh K. Gaharwar[1,2,*]*

[1]Department of Biomedical Engineering, Texas A&M University, College Station, TX 77841, USA
[2]Department of Materials Science and Engineering, Texas A&M University, College Station, TX 77841, USA
Corresponding author: Prof. Roland Kaunas (rkaunas@tamu.edu); Prof. A. K. Gaharwar (gaharwar@tamu.edu)

Keywords: Nanocomposite, hydroxyapatite nanoparticles, hydrogels, tissue engineering, mechanical properties.

Abstract

Nanocomposite biomaterials are extensively investigated for cell and tissue engineering applications due their unique physical, chemical and biological characteristics. Here, we investigated the mechanical, rheological, and degradation properties of photocrosslinkable and elastomeric nanocomposite hydrogels from nanohydroxyapatite (nHAp) and gelatin methacryloyl (GelMA). The addition of nHAp resulted in a significant increase in mechanical stiffness and physiological stability. Cells readily adhere and proliferate on the nanocomposite surfaces. Cyclic stretching of cells on the elastomeric nanocomposites revealed that nHAp elicited a stronger alignment response in the direction of strain. *In vitro* studies highlight enhanced bioactivity of nanocomposites as determined by alkaline phosphate (ALP) activity. Overall, the elastomeric and photocrosslinkable nanocomposite hydrogels can be used for minimally invasive therapy for bone regeneration.

INTRODUCTION:

Over the past decade, regenerative medicine has witnessed tremendous advances owing to an increase in clinical demand for bioactive materials to repair and regenerate damaged bone tissue.[1, 2] Though bone injuries and defects may seem relatively simple to treat with conventional methods, treatment of complex fractures or pathological conditions in the elderly is a challenge. Current treatment involves replacement of damaged tissue with bone grafts, usually involving metallic pins, rods or plates that act as support systems. These surgical methods are far from ideal as they may require extended healing time and potentially multiple surgeries.[3] Recent bone tissue engineering approaches focus on mimicking the structure and chemical composition of tissues by providing an appropriate extracellular matrix (ECM) environment to activate cellular functions.[4-7]

In that regard, bioresorbable nanocomposites have shown strong promise as an artificial ECM. A range of inorganic nanoparticles have been investigated for bone tissue engineering applications including hydroxyapatite, β-tricalcium phosphate, bioactive glasses, β-wollastonite, A-W (Apatite-Wollastonite) glass ceramic, graphene, and nanosilicates.[8-10] However, these nanomaterials have some disadvantages including their brittle nature, poor processing ability, and lack of control over degradation and dissolution kinetics. To overcome these disadvantages, these inorganic nanoparticles are combined with polymeric networks to obtain polymeric nanocomposites.[11-13] Within the polymeric chains, these nanoparticles interact physically or covalently to form a crosslinked network with multiple functionalities.[14-16]

Among these nanomaterials, nanohydroxyapatite (nHAp) has been combined with various hydrophobic polymers to fabricate nanocomposite scaffolds. Mineralized tissues such as bone are composed of inorganic mineral (nHAp ~ 69 wt%) and an organic component containing predominantly collagen.[6, 17] Thus, nHAp has been extensively investigated for a range of biomedical applications including bone tissue engineering, dental fillers, and drug delivery.[18-22] By combining nHAp with a polymeric network, bioactive nanocomposites with well-defined cell matrix interactions can be

designed.[23, 24] For example, Becker *et al.* showed that combining nHAp with biodegradable poly(propylene fumarate)-co-poly(caprolactone) (PPF-co-PCL) enhances osteoblast adhesion and production of mineralized ECM.[25] In another study, porous scaffolds were fabricated from poly(L-lactide) (PLLA) grafted nHAp that enhance bone regeneration in critical size defects.[26] Similarly, a multi-component scaffold composed of chitosan, poly(lactic acid) and nHAp displays improved mechanical resilience.[27] Human bone marrow stem cells (hMSC) seeded on nHAp- bacterial cellulose nanocomposites revealed augmented expression of osteo-related proteins such as osteopontin, osteocalcin, and bone sialoprotein.[28]

The elastomeric properties of nanocomposite hydrogels allow cyclic strain to be applied to the attached cells, which may provide an osteogenic cue. Large magnitude tensile strain (~0.1 strain) stimulate *in vivo* bone formation.[29] Cyclic tensile strain of mesenchymal stem cells (MSC), osteoblasts, and periosteal cells in 2-D culture at these magnitudes also enhance cell proliferation and upregulate bone marker genes.[30-32] More recent work has shown that human MSCs cultured in 3-D collagen hydrogels also respond to cyclic strain in a pro-osteogenic manner.[33] Cell morphological changes in response to cyclic strain depend on hydrogel stiffness[34, 35]; our study is the first to test this concept with hydrogels stiffened using nanoparticles.

Recently, a few approaches have focused on engineering bioactive hydrogels by combining nHAp with hydrophilic polymers such as poly(ethylene glycol) (PEG)[36], polyacrylamide (PAAm)[37], poly(vinyl alcohol) (PVA)[38], alginate[39], carrageenan[40], gelatin[37] and collagen[17]. This variety of polymers has expanded the use of nHAp in nanocomposite hydrogels, allowing for tailored functionality.[41, 42] However, most of these nanocomposite scaffolds are designed for use as scaffolds and very few studies focus on engineering nanocomposite hydrogels that can be easily injected. Injectable hydrogels are emerging as an effective tool for delivery of a range of moieties including stem cells, gene delivery vectors, and drugs for various clinical treatments.[43-46] These injectable networks can be shaped or casted into various sizes and shapes useful for minimally invasive therapies to facilitate bone repair,

remodeling, and regeneration. Additionally, the effect of addition of nHAp on osteogenic differentiation of cells has not been investigated.

Here, we engineer a photocrosslinkable and elastomeric nanocomposite hydrogel from nHAp and denatured collagen (gelatin). The addition of nHAp to hydrogel networks increased the mechanical stiffness and physiological stability due to strong nanoparticle-polymer interactions. The photocrosslinkable process also avoids the use of toxic crosslinkers, allowing injection of the nanocomposite to the defect site using a minimally invasive approach. Moreover, facile encapsulation of cells within the hydrogel network resulted in high cell viability and functionality. The elastomeric characteristics of nanocomposite hydrogels render it useful for understanding cellular behavior under dynamic mechanical loading. Moreover, the presence of nHAp within the hydrogel networks supported the ostegenic differentiation of seeded preosteoblasts. The proposed nanoengineered system can be used to deliver cells to support regeneration of the damaged bone tissue at non-load bearing site. It is expected that bioactive hydrogel carriers will enhance cell survival and retention at the injury site.

MATERIALS AND METHODS

Gelatin Methacryloyl (GelMA) Synthesis: Gelatin (type A), hydroxyapatite nanopowder (nHAp) and methacrylic anhydride (MA) were obtained from Sigma-Aldrich, USA. Methacrylation of gelatin was performed using previously reported method to obtain gelatin methacryloyl (GelMA) with 80% methacrylation degree.[47] Nanocomposite prepolymer solutions were prepared by combining nHAp (0, 0.5, 1 and 2.5 wt%), GelMA (5 wt%) and photoinitiator (0.5 wt% IRGACURE® 2959 obtained from Ciba Specialty Chemical, USA). Chemically crosslinked hydrogels were obtained by subjecting the prepolymer solutions to UV (320-500nm) using a high intensity UV lamp (Omnicure S200, Lumen Dynamics, Canada) for 90 seconds at an intensity of 1.44 W/cm^2. The nanocomposites were soaked in PBS for six hours to remove uncrosslinked GelMA and nHAp.

Structural characterization of nanocomposite hydrogels: Crystalline structure of nHAp was investigated using x-ray diffraction (XRD) using Bruker D8 Advance Diffractometer using Cu K_α= 1.54Å. The crystalline size, $t_{(hkl)}$ of nHAp was determined using the Debye-Scherrer equation. Morphological features of the nHAp were investigated using JEOL 2100 transmission electron microscopy (TEM) on carbon-coated copper grid. Zeta potentials of GelMA, nHAp, and GelMA-nHAp prepolymers were determined using Zetasizer Nano Z (Malvern Instruments, UK). Attenuated Total Reflectance (ATR) of lyophilized nanocomposite hydrogels was investigated by FTIR spectrometer (Vector 22, Bruker Optics). The surface morphology and energy dispersive spectra (EDS) of hydrogels were determined using FEI Quanta 600 scanning electron microscopy (SEM) at 10kV. ImageJ (NIH) software was used to analyze the pore diameters and wall thickness.

Physical characterization of nanocomposite hydrogels: The mechanical properties of the nanocomposites were investigated with uniaxial and cyclic compression tests (1 mm/min strain rate) using the MTESTQuattro (ADMET, USA). A MCR Rheometer (Anton Paar, USA) was used to evaluate the viscoelastic behavior of nanocomposite. The viscoelastic property of nanocomposite hydrogels was determined using stress sweep at 10 rad/sec from 0.1-10 Pa stress. Gelation kinetics of prepolymer solutions were determined via UV rheology; the light source was turned on at 30 sec and kept on until storage modulus (G') plateaus were observed (approximately 180 sec). The degradation characteristic of the nanocomposite hydrogel was determined through enzymatic degradation by incubating them in a freshly prepared collagenase (Worthington Biochemicals, USA) solution at a concentration of 2.5 units/mL in PBS at 37˚C. Hydrogel weight loss was examined until their complete degradation, and the percent mass remaining was calculated.

In vitro cell studies: Cell culture was performed using NIH MC3T3 E1-4 mouse preosteoblasts (ATCC, USA) in αMEM growth media, which was supplemented with 10% fetal bovine serum and 1% penicillin/streptomycin (100U/100µg/mL). All cell culture reagents were obtained from Life Technologies, USA. To investigate cell behavior in the presence of nHAp, preosteoblasts were seeded

into a 96-well plate (8000 cells/well) and after 6 hours, media was replaced with media containing 0, 50, 100 and 250 μg/mL of nHAp. After 0, 1, and 2 days, cell viability was determined using Calcein AM and Ethidium homodimer (Santa Cruz Biotechnology Inc., USA). The cells were incubated with Calcein AM and Ethidium homodimer reagents for 30 minutes at 37˚C and then fixed with glutaraldehyde (2%) for 10-15 minutes before staining with DAPI (300 nM). Epifluorescence microscope (TE2000-S, Nikon, USA) was used to image the cells. To investigate cell behavior on nanocomposite hydrogels, cylindrical samples (15mm diameter and 400μm thickness) were placed in 24 well plates and sterilized using UV light for 12 hours. After sterilization, preosteoblasts were seeded onto the hydrogels (20,000 cells/well) and after 3 and 7 days samples were fixed with 2% glutaraldehyde (90 minutes) for SEM imaging. The cell-seeded scaffolds were subjected to serial dehydration with a stepwise increase in ethanol concentration (20, 50, 70, 80, 90 and 100%). Critical point drying of the samples was facilitated by adding 200μL of Hexamethyldisilaxane (HMDS) and the samples were kept in the fume hood overnight for drying before using for SEM imaging.

Cyclic Stretching Experiment: Silicone rubber stretch chambers embedded with two small sponges to anchor the ends of the hydrogel (4 cm^2, STREX, Japan) were sterilized with 70% ethanol followed by UV radiation. The stretch chambers were initially surface-coated with collagen (0.25 mg/cm^2) by incubating 400 μL of 2.5 mg/mL rat-tail collagen type-I (Corning) and PBS and allowing the solution to evaporate. GelMA or GelMA-nHAp polymer solution was then added to the chambers and subjected to UV radiation to form 1.25 mm-thick crosslinked 3-D gels. Preosteoblasts were seeded at a cell density of 2.5×10^3 $cells/cm^2$ on the gel surface and allowed to spread overnight. Media was replaced with fresh media just prior to cyclic uniaxial stretching (0.08 strain, 1 Hz) using two linear motors (Zaber, Canada) in a humidified 5% CO_2/95% air incubator as previously described.[34, 35] In parallel, similar steps were taken with static controls. After 6 hours of cyclic stretching, static control and stretched cells were immediately rinsed with PBS, fixed with 4% formaldehyde, and permeabilized with 0.5% Triton X-100. Cells were then stained with Alexa Fluor 488 phalloidin (Life Technologies) and propidium iodine (PI,

Life Technologies) to detect actin stress fibers and the nuclei, respectively. Images were captured on an upright microscope (Nikon FN1) using a laser scanning confocal head attachment (Nikon C1) and a 60X water-dipping objective. Images were analyzed using a custom algorithm in MATLAB (the MathWorks, Natick, MA) to quantify the angular distribution of stress fibers (SF) for each cell imaged as previously described. [35] To quantify cell alignment, cell outlines obtained by image thresholding were fit with ellipses to quantify orientation angles θ using NIH ImageJ software that were summarized with the order parameter $S = \langle \cos 2\theta \rangle$, where θ is the angle of the major axis relative to the major axis of the stretch chamber. Values of -1 or 1 indicate cells are uniformly oriented perpendicular or parallel to the direction of stretch, while a value of 0 indicates there is no preferred orientation.

In vitro Differentiation: Preosteoblast metabolic activity was determined using AlamarBlue assay (Thermo Scientific, USA) according to the manufacturer's protocol. Nanocomposite hydrogels (6mm diameter, 400 μm thickness) in a 96-well plate were seeded with 10,000 cells/well in normal and osteoconductive media (50 μM ascorbic acid and 10 mM β-glycerophosphate supplemented in normal media). The alkaline phosphatase (ALP) staining was performed on Days 3, and 7 using nitro-blue tetrazolium/indolyl phosphate (NBIT/BCIP) (Thermo Scientific, USA). Cells were incubated with 0.25ml of NBIT/BCIP for 30 minutes then imaged using a stereomicroscope (Amscope, USA) after extensive washing. For quantitative analysis, ALP was extracted from cells and subjected to mild shaking at 4˚C for 1 hour followed by centrifugation at 2500x for 10 minutes. Cell lysates were collected in 96 - well plate and equal volume of p-nitrophenylphosphate (PNPP) (Sigma-Aldrich, USA) substrate was added and incubated at 37˚C for 1 hour to allow cleavage of the chromogenic substrate. Absorbance was recorded at an OD of 405nm.

Statistical Analysis: The experimental data were presented as mean and standard deviations (n=5 or 6). GraphPad Prism 5 was used to perform statistical analysis using non-parametric tests and one-way

analysis of variance (ANOVA). Tukey's post-hoc analysis was used for pairwise comparisons and the statistical significance was defined as *p <0.05, **p <0.01, ***p <0.005.

RESULTS AND DISCUSSION

Synthesis of Nanohydroxyapatite-Gelatin Nanocomposites:

The size, morphology, and crystalline structure of nHAp were investigated through TEM and XRD analysis. TEM analysis of nanoparticles revealed circular morphology of the nanoparticles with an average diameter of 54±13 nm **(Figure 1a).** XRD pattern of nHAp was consistent with the phases listed by International Centre for Diffraction Data (ICDD) database**.** The XRD pattern indicates presence of (002), (211), (300), (202), (130), (002), (222) and (213) characteristic plane **(Figure 1b).** The XRD pattern of nHAp was consistent with the phases listed by International Centre for Diffraction Data (ICDD) database and match with JCPDS card (09-0432). The crystalline size of the nanoparticles as calculated from the Debye-Scherrer formula was found to be 16±3 nm. This indicates the crystalline nature of the nHAp particles. The effect of nHAp on cells was investigated by evaluating the cell viability and cell shape **(Figure 1c)**. No significant change in cell viability or cell shape was observed in presence of nHAp (250 μg/mL), indicating high cytocompatibility of nanoparticles.

The nanocomposite hydrogels were obtained by combining nHAp with GelMA prepolymer solution and subjecting it to UV radiation to obtain fully crosslinked network **(Figure 2a)**. The presence of nHAp in the GelMA hydrogel after crosslinking was determined using FTIR **(Figure 2b).** Gelatin shows characteristic peaks of N-H stretching at 3276 cm^{-1}, C-H stretching at 2977 and 2880 cm^{-1}, amide I, II and III bands at 1625, 1533 and 1246 cm^{-1}, respectively and C-H deformation band at 1390 cm^{-1}. After methacrylation of gelatin, the amide peak shifted from 1625 cm^{-1} to 1631 cm^{-1}, indicating the formation of amide linkage. C-O-C stretching from methacrylic group appeared at 1029 cm^{-1}. nHAp spectra showed peaks at 1091, 1041 and 962 cm^{-1} corresponding to PO_4^{3-} (v3) vibrational band and three peaks at 627, 600 and 566 cm^{-1} corresponding to PO_4^{3-} (v4) vibrational band. PO_4^{3-} (v1) band was

observed in the region of 473 and 439 cm^{-1}. A hydroxyl band was observed at 627 cm^{-1}. CO_3^{2-} (v3) vibrational bands were centered at 1655, 1461 and 1413 cm^{-1}. The spectra of nanocomposite confirm the presence of nHAp and GelMA.

To understand the physical interactions between nHAp and GelMA, the electrophoretic mobility (zeta potential) was determined. The zeta potentials of nHAp and GelMA prepolymer solutions were observed to be -8.4±0.7 mV and -15±0.7 mV, respectively. The addition of 0.5, 1 and 2.5% nHAp to prepolymer solution resulted in zeta potential of -14.2±0.5 mV, -14.1±0.1 mV to -13.1±0.2 mV respectively **(Figure 2c)**. As the zeta potential data is dominated by GelMA, this data indicates that surface of nHAp is covered by GelMA. No significant aggregation of nanoparticles was observed and the prepolymer solution seemed stable. This is attributed to strong physical interactions between nHAp and GelMA, due to high surface to volume ratio of nHAp compared to relatively large micron-sized particles. The gelation kinetics of nanocomposite system was determined using UV rheology. The pre-polymer solutions were subjected to UV radiations and the storage (*G'*) and loss (*G''*) moduli were determined to monitor the crosslinking process **(Figure 2d)**. The results indicate that crosslinking starts in GelMA upon UV exposure and storage modulus reaches plateau within 60 seconds of UV exposure. For GelMA + 2.5% nHAp, a delay in the crosslinking process was observed. This might be attributed to the ability of nHAp to adsorb UV. The storage modulus of the nanocomposite hydrogel was significantly higher compared to the GelMA hydrogels.

Structural and Mechanical Characterization of Photocrosslinked Nanocomposite Hydrogels

The effect of nHAp addition on structure and pore size of the GelMA hydrogels were investigated using SEM. The porous network of hydrogels enables nutrient diffusion and facilitates cell proliferation. In the GelMA hydrogels, a highly interconnected porous network was observed corresponding to previously reported results.[48] With the addition of nHAp, the pore size increased without significantly affecting the interconnectivity of the porous network **(Figure 3a)**. A two-fold

increase in pore size was due to addition of 2.5% nHAp in the nanocomposite hydrogel compared to the GelMA hydrogel. Additionally, no aggregation of nHAp was observed indicating the uniform distribution of nHAp within the hydrogel network. This increase in pore size due to the addition of nHAp corresponds to the previously published studies.[36] Interestingly, an increase in pore wall thickness was also observed with an increase in nHAp concentration **(Figure 3b)**. It might be possible that addition of nHAp reduces the crosslinking density of GelMA as nHAp can hinder the kinetic chain growth and result in larger pores with thicker walls. Earlier reports also support this hypothesis.[49, 50] Moreover, due to its crystalline nature, nHAp can also absorb UV radiation that can also interfere with the polymerization process. The energy dispersive spectra (EDS) of crosslinked network indicate the presence of nHAp in the nanocomposite network as shown by the presence of Calcium (Ca) and Phosphorus (P) peaks. The increase in nHAp concentration results in an increase in the intensity of Ca and P peaks.

The addition of nHAp was expected to increase the network's mechanical stiffness due to physical reinforcement. Cyclic compression was performed to evaluate the mechanical properties of the nanocomposite scaffolds. The addition of nHAp significantly increased the modulus and ultimate stress. A two-fold increase in modulus and a four-fold increase in ultimate stress were observed with the addition of 2.5% nHAp to GelMA **(Figure 4a)**. The energy dissipated or the area under the stress-strain curve was calculated for each scaffold. A four-fold increase in the energy dissipated was also observed with the addition of 2.5% nHAp; 2.60 ± 0.61 kJ/m^3 and 10.85 ± 2.09 kJ/m^3 respectively. With the increase in stiffness and strength of the scaffold with addition of nHAp, it is expected that there be an increase in the energy lost when the scaffold is compressed to 90% strain. Previous studies also have shown the inclusion of nanoparticles to increase mechanical properties of hydrogel network. [36, 48] Although the addition of nHAp to GelMA significantly enhances the mechanical stiffness of hydrogel network, the nanocomposite is not strong enough to be used in load-bearing region. We expect that this injectable nanocomposite system will be used for non-load bearing regions or in conjunction with stress-

shielding devices such as bone plates or external fixations. The primary function of the injectable nanocomposite will be to delivery cells or therapeutics and provide osteoconductive microenvironment to support bone regeneration.

The degradation rates of the nanocomposite hydrogels were observed using collagenase solution (2.5 units/mL) at 37°C. Since GelMA contains denatured collagen, it fully degraded in collagenase in 12-16 hours **(Figure 4b)**, which was comparable to previous results.[48] The collagenase solution was able to penetrate the hydrogel networks because of their interconnected porous structures. The stability of the hydrogel networks was increased by the addition of nHAp, which allowed for a decrease in the degradation rate.

Nanocomposite Hydrogels Support Cell Adhesion, Spreading and Differentiation

In order to be considered for biomedical applications, a scaffold must support cell adhesion and promote cell proliferation. Since gelatin is denatured collagen, it contains RGD sequences that allow for integrin mediated cell adhesion. In addition, nHAp are chemically and structurally similar to the mineral phase of native bone, and can enhance the bone-bonding ability of the hydrogel scaffolds. To investigate cell adhesion and spreading, preosteoblast cells were seeded on the nanocomposite scaffolds. After 3 and 7 days, SEM images of the cell-seeded scaffold were taken to analyze cell adhesion and spreading. Results showed that cells attach and spread on the nanocomposite surface **(Figure 5a)**. The metabolic activity of seeded cells was monitored in normal and osteoconductive media. No significant difference in metabolic activity was observed between GelMA and nanocomposite scaffolds (**Figure 5b**). A slight increase in metabolic activity of cells was observed on the nanocomposite with higher nHAp concentration on Day 7 and 14 in normal media conditions.

Cyclic Stretch-Induced Cell Alignment on Nanocomposite Hydrogels

As an assessment of the effect of addition of nHAp on cell responsiveness to cyclic tensile strain (0.08 strain, 1Hz), we quantified stretch-induced alignment of non-confluent preosteoblasts cultured on GelMA and GelMA-2.5% nHAp hydrogels (**Figure 6a**). Circular histograms of stress fiber orientation distributions clearly indicate stress fiber alignment parallel to the direction of strain as compared to a lack of alignment in static controls (**Figure 6b**). While alignment was apparent on both GelMA and GelMA-2.5% nHAp hydrogels, the extent of stress fiber alignment was noticeably greater in the hydrogels containing nHAp. The extent of cell alignment, as quantified by the order parameter, was negligible for both GelMA (0.17 ± 0.13) and GelMA-2.5% nHAp (0.20 ± 0.11) static control groups (**Figure 6c**). Cyclic stretching increased the order parameters for GelMA (0.52 ± 0.10) and GelMA-2.5% nHAp (0.67 ± 0.07), but this was statistically significant only for the nHAp-containing gels. As compared to 3D collagen hydrogels where cells and collagen fibrils are often co-aligned parallel with the direction of strain[51], the GelMA hydrogels used here have no fibrils and thus alignment did not occur as a result of contact guidance along aligned fibrils. These results are consistent with our previous report stretching cells on collagen hydrogels.[34, 35] Previous reports have demonstrated that cells align in the direction of lowest strain on silicone rubber and polyacrylamide substrates with an elastic modulus of 50kPa, while no alignment is observed when stretching the cells on substrates softer than 11kPa.[52, 53] While we also observed greater alignment on the stiffer GelMA-2.5% nHAp hydrogel (5kPa vs. 2 kPa for GelMA), the direction of alignment was in the direction of greatest strain and occurred at an elastic modulus below 11kPa. Future experiments will focus on the effects of nHAp on stretch-induced cell functions, including proliferation and osteogenic response.

Enhanced Osteogenic Response of Preosteoblasts Seeded on Nanocomposites

By controlling biochemical and physical cues in the engineered ECM, it is possible to regulate or enhance outcomes that facilitate tissue regeneration. The addition of nHAp to GelMA increases the mechanical properties but also provides calcium reservoir to modulate the metabolic response of

preosteoblast. The effects of nHAp on early osteogenic responses of seeded preosteoblast were monitored by qualitative and quantitative assessment of the presence and activity of ALP. As an early marker for osteogenesis, ALP production was monitored on days 3 and 7. Qualitative assessment showed a significant increase in the presence of ALP in the 2.5% nHAp composite scaffold in comparison to the control GelMA scaffold in both the normal and osteoconductive media (**Figure 7**). Specifically, the number of ALP stained cells (purple stain) increased with the addition of nHAp. Additionally, an increase in ALP stained cells was observed on day 7 compared to day 3. Further quantitative analysis supported this by showing a significant increase in ALP activity on the 2.5% nHAp scaffold.

CONCLUSIONS

Overall, we synthesized photocrosslinkable and elastomeric nanocomposite hydrogels from nanohydroxyapatite (nHAp) and gelatin methacrylate (GelMA). We investigated the effect of nHAp addition on mechanical, rheological, and degradation properties. The results indicate significant increase in mechanical stiffness and physiological stability due to the addition of nHAp. *In vitro* cell studies indicate that the nanocomposite system supports cell adhesion, and proliferation. The nanocomposites loaded with nHAp show enhanced interaction with cells under dynamic loading conditions. Furthermore, the addition of nHAp significantly enhances the bioactivity of nanocomposite as determined by alkaline phosphate (ALP) activity. The photocrosslinking ability of nanocomposites renders its utility for minimally invasive therapies.

ACKNOWLEDGMENT

LC would like to acknowledge financial support from Texas A&M University Graduate Diversity Fellowship. This work is partly supported by NIH AR066033 and NSF CBET-1264848 to RK.

REFERENCES:

1. Amini, A. R.; Laurencin, C. T.; Nukavarapu, S. P. Bone Tissue Engineering: Recent Advances and Challenges. *Critical reviews in biomedical engineering* 2012, 40, 363-408.
2. Langer, R.; Vacanti, J. P. Tissue engineering. *Science* 1993, 260, 920-926.
3. Holzwarth, J. M.; Ma, P. X. Biomimetic nanofibrous scaffolds for bone tissue engineering. *Biomaterials* 2011, 32, 9622-9629.
4. Kim, B.-S.; Mooney, D. J. Development of biocompatible synthetic extracellular matrices for tissue engineering. *Trends in Biotechnology* 1998, 16, 224-230.
5. Bose, S.; Roy, M.; Bandyopadhyay, A. Recent advances in bone tissue engineering scaffolds. *Trends in biotechnology* 2012, 30, 546-554.
6. Zhou, H.; Lee, J. Nanoscale hydroxyapatite particles for bone tissue engineering. *Acta Biomaterialia* 2011, 7, 2769-2781.
7. Liu, Y.; Lim, J.; Teoh, S.-H. Review: development of clinically relevant scaffolds for vascularised bone tissue engineering. *Biotechnology advances* 2013, 31, 688-705.
8. Hench, L. L. Bioceramics: from concept to clinic. *J. Am. Ceram. Soc.* 1991, 74, 1487-1510.
9. Hench, L. L.; Polak, J. M. Third-Generation Biomedical Materials. *Science* 2002, 295, 1014-1017.
10. Chimene, D.; Alge, D. L.; Gaharwar, A. K. Two‐Dimensional Nanomaterials for Biomedical Applications: Emerging Trends and Future Prospects. *Advanced Materials* 2015, DOI: 10.1002/adma.201502422.
11. Carrow, J. K.; Gaharwar, A. K. Bioinspired Polymeric Nanocomposites for Regenerative Medicine. *Macromolecular Chemistry and Physics* 2015, 216, 248-264.
12. Kerativitayanan, P.; Carrow, J. K.; Gaharwar, A. K. Nanomaterials for Engineering Stem Cell Responses. *Advanced healthcare materials* 2015, 4, 1600–1627.
13. Gaharwar, A. K.; Peppas, N. A.; Khademhosseini, A. Nanocomposite hydrogels for biomedical applications. *Biotechnology and bioengineering* 2014, 111, 441-453.
14. Schexnailder, P.; Schmidt, G. Nanocomposite polymer hydrogels. *Colloid and Polymer Science* 2009, 287, 1-11.
15. Kerativitayanan, P.; Gaharwar, A. K. Elastomeric and mechanically stiff nanocomposites from poly (glycerol sebacate) and bioactive nanosilicates. *Acta biomaterialia* 2015, 26, 34-44.
16. Gaharwar, A. K.; Rivera, C.; Wu, C.-J.; Chan, B. K.; Schmidt, G. Photocrosslinked nanocomposite hydrogels from PEG and silica nanospheres: structural, mechanical and cell adhesion characteristics. *Materials Science and Engineering: C* 2013, 33, 1800-1807.
17. Villa, M. M.; Wang, L.; Huang, J.; Rowe, D. W.; Wei, M. Bone tissue engineering with a collagen–hydroxyapatite scaffold and culture expanded bone marrow stromal cells. *Journal of Biomedical Materials Research Part B: Applied Biomaterials* 2015, 103, 243-253.
18. Bohner, M. Calcium orthophosphates in medicine: from ceramics to calcium phosphate cements. *Injury* 2000, 31, Supplement 4, D37-D47.
19. Dorozhkin, S. Calcium orthophosphate-based biocomposites and hybrid biomaterials. *J Mater Sci* 2009, 44, 2343-2387.
20. Ginebra, M. P.; Espanol, M.; Montufar, E. B.; Perez, R. A.; Mestres, G. New processing approaches in calcium phosphate cements and their applications in regenerative medicine. *Acta Biomaterialia* 2010, 6, 2863-2873.
21. Wagoner Johnson, A. J.; Herschler, B. A. A review of the mechanical behavior of CaP and CaP/polymer composites for applications in bone replacement and repair. *Acta Biomaterialia* 2011, 7, 16-30.
22. Ginebra, M. P.; Traykova, T.; Planell, J. A. Calcium phosphate cements as bone drug delivery systems: A review. *Journal of Controlled Release* 2006, 113, 102-110.

23. Balazs, A. C.; Emrick, T.; Russell, T. P. Nanoparticle Polymer Composites: Where Two Small Worlds Meet. *Science* 2006, 314, 1107-1110.
24. Li, X.; Wang, L.; Fan, Y.; Feng, Q.; Cui, F.-Z.; Watari, F. Nanostructured scaffolds for bone tissue engineering. *Journal of Biomedical Materials Research Part A* 2013, 101A, 2424-2435.
25. Becker, J.; Lu, L.; Runge, M. B.; Zeng, H.; Yaszemski, M. J.; Dadsetan, M. Nanocomposite bone scaffolds based on biodegradable polymers and hydroxyapatite. *Journal of Biomedical Materials Research Part A* 2014.
26. Zhang, P.; Hong, Z.; Yu, T.; Chen, X.; Jing, X. In vivo mineralization and osteogenesis of nanocomposite scaffold of poly (lactide-co-glycolide) and hydroxyapatite surface-grafted with poly (L-lactide). *Biomaterials* 2009, 30, 58-70.
27. Cai, X.; Tong, H.; Shen, X.; Chen, W.; Yan, J.; Hu, J. Preparation and characterization of homogeneous chitosan–polylactic acid/hydroxyapatite nanocomposite for bone tissue engineering and evaluation of its mechanical properties. *Acta biomaterialia* 2009, 5, 2693-2703.
28. Fang, B.; Wan, Y.-Z.; Tang, T.-T.; Gao, C.; Dai, K.-R. Proliferation and osteoblastic differentiation of human bone marrow stromal cells on hydroxyapatite/bacterial cellulose nanocomposite scaffolds. *Tissue Engineering Part A* 2009, 15, 1091-1098.
29. Loboa, E. G.; Fang, T. D.; Warren, S. M.; Lindsey, D. P.; Fong, K. D.; Longaker, M. T.; Carter, D. R. Mechanobiology of mandibular distraction osteogenesis: experimental analyses with a rat model. *Bone* 2004, 34, 336-343.
30. Kanno, T.; Takahashi, T.; Ariyoshi, W.; Tsujisawa, T.; Haga, M.; Nishihara, T. Tensile mechanical strain up-regulates Runx2 and osteogenic factor expression in human periosteal cells: implications for distraction osteogenesis. *Journal of oral and maxillofacial surgery* 2005, 63, 499-504.
31. Fong, K. D.; Nacamuli, R. P.; Loboa, E. G.; Henderson, J. H.; Fang, T. D.; Song, H. M.; Cowan, C. M.; Warren, S. M.; Carter, D. R.; Longaker, M. T. Equibiaxial tensile strain affects calvarial osteoblast biology. *Journal of Craniofacial Surgery* 2003, 14, 348-355.
32. Koike, M.; Shimokawa, H.; Kanno, Z.; Ohya, K.; Soma, K. Effects of mechanical strain on proliferation and differentiation of bone marrow stromal cell line ST2. *Journal of bone and mineral metabolism* 2005, 23, 219-225.
33. Charoenpanich, A.; Wall, M. E.; Tucker, C. J.; Andrews, D. M.; Lalush, D. S.; Dirschl, D. R.; Loboa, E. G. Cyclic tensile strain enhances osteogenesis and angiogenesis in mesenchymal stem cells from osteoporotic donors. *Tissue Engineering Part A* 2013, 20, 67-78.
34. Tondon, A.; Hsu, H.-J.; Kaunas, R. Dependence of cyclic stretch-induced stress fiber reorientation on stretch waveform. *Journal of biomechanics* 2012, 45, 728-735.
35. Tondon, A.; Kaunas, R. The direction of stretch-induced cell and stress fiber orientation depends on collagen matrix stress. *PloS one* 2014, 9, e89592.
36. Gaharwar, A. K.; Dammu, S. A.; Canter, J. M.; Wu, C.-J.; Schmidt, G. Highly extensible, tough, and elastomeric nanocomposite hydrogels from poly (ethylene glycol) and hydroxyapatite nanoparticles. *Biomacromolecules* 2011, 12, 1641-1650.
37. Li, Z.; Mi, W.; Wang, H.; Su, Y.; He, C. Nano-hydroxyapatite/polyacrylamide composite hydrogels with high mechanical strengths and cell adhesion properties. *Colloids and Surfaces B: Biointerfaces* 2014, 123, 959-964.
38. Poursamar, S. A.; Azami, M.; Mozafari, M. Controllable synthesis and characterization of porous polyvinyl alcohol/hydroxyapatite nanocomposite scaffolds via an in situ colloidal technique. *Colloids and Surfaces B: Biointerfaces* 2011, 84, 310-316.
39. Zhang, J.; Wang, Q.; Wang, A. In situ generation of sodium alginate/hydroxyapatite nanocomposite beads as drug-controlled release matrices. *Acta Biomaterialia* 2010, 6, 445-454.
40. Liu, H.; Cheng, J.; Chen, F.; Hou, F.; Bai, D.; Xi, P.; Zeng, Z. Biomimetic and cell-mediated mineralization of hydroxyapatite by carrageenan functionalized graphene oxide. *ACS applied materials & interfaces* 2014, 6, 3132-3140.

41. Peppas, N. A.; Hilt, J. Z.; Thomas, J. B. *Nanotechnology in Therapeutics: Current Technology and Applications*. Horizon Bioscience: Norfolk, UK, 2007.
42. Lowman, A. M.; Dziubla, T. D.; Bures, P.; Peppas, N. A. Structural and Dynamic Response of Neutral and intelligent Networks in Biomedical Environments. In *Molecular and Cellular Foundations of Biomaterials*, Peppas, N. A.; Sefton, M. V., Eds. Academic Press: New York, 2004; Vol. 29, pp 75-130.
43. Seo, B.-B.; Choi, H.; Koh, J.-T.; Song, S.-C. Sustained BMP-2 delivery and injectable bone regeneration using thermosensitive polymeric nanoparticle hydrogel bearing dual interactions with BMP-2. *Journal of Controlled Release* 2015, 209, 67-76.
44. Paul, A.; Hasan, A.; Kindi, H. A.; Gaharwar, A. K.; Rao, V. T.; Nikkhah, M.; Shin, S. R.; Krafft, D.; Dokmeci, M. R.; Shum-Tim, D. Injectable graphene oxide/hydrogel-based angiogenic gene delivery system for vasculogenesis and cardiac repair. *ACS nano* 2014, 8, 8050-8062.
45. Peak, C. W.; Carrow, J. K.; Thakur, A.; Singh, A.; Gaharwar, A. K. Elastomeric Cell-Laden Nanocomposite Microfibers for Engineering Complex Tissues. *Cellular and Molecular Bioengineering* 2015, 8, 404-415.
46. Short, A. R.; Koralla, D.; Deshmukh, A.; Wissel, B.; Stocker, B.; Calhoun, M.; Dean, D.; Winter, J. O. Hydrogels that allow and facilitate bone repair, remodeling, and regeneration. *Journal of Materials Chemistry B* 2015, 3, 7818-7830.
47. Nichol, J. W.; Koshy, S.; Bae, H.; Hwang, C. M.; Yamanlar, S.; Khademhosseini, A. Cell-laden microengineered gelatin methacrylate hydrogels. *Biomaterials* 2010, 31, 5536-5544.
48. Xavier, J. R.; Thakur, T.; Desai, P.; Jaiswal, M. K.; Sears, N.; Cosgriff-Hernandez, E.; Kaunas, R.; Gaharwar, A. K. Bioactive Nanoengineered Hydrogels for Bone Tissue Engineering: A Growth-Factor-Free Approach. *ACS nano* 2015, 9, 3109-3118.
49. Burdick, J. A.; Lovestead, T. M.; Anseth, K. S. Kinetic chain lengths in highly cross-linked networks formed by the photoinitiated polymerization of divinyl monomers: A gel permeation chromatography investigation. *Biomacromolecules* 2003, 4, 149-156.
50. Khanlari, A.; Detamore, M. S.; Gehrke, S. H. Increasing cross-linking efficiency of methacrylated chondroitin sulfate hydrogels by copolymerization with oligo (ethylene glycol) diacrylates. *Macromolecules* 2013, 46, 9609-9617.
51. Roby, T.; Olsen, S.; Nagatomi, J. Effect of sustained tension on bladder smooth muscle cells in three-dimensional culture. *Annals of biomedical engineering* 2008, 36, 1744-1751.
52. Faust, U.; Hampe, N.; Rubner, W.; Kirchgessner, N.; Safran, S.; Hoffmann, B.; Merkel, R. Cyclic stress at mHz frequencies aligns fibroblasts in direction of zero strain. *PLoS One* 2011, 6, e28963.
53. Throm Quinlan, A. M.; Sierad, L. N.; Capulli, A. K.; Firstenberg, L. E.; Billiar, K. L. Combining Dynamic Stretch and Tunable Stiffness to Probe Cell Mechanobiology In Vitro. *PLoS ONE* 2011, 6, e23272.

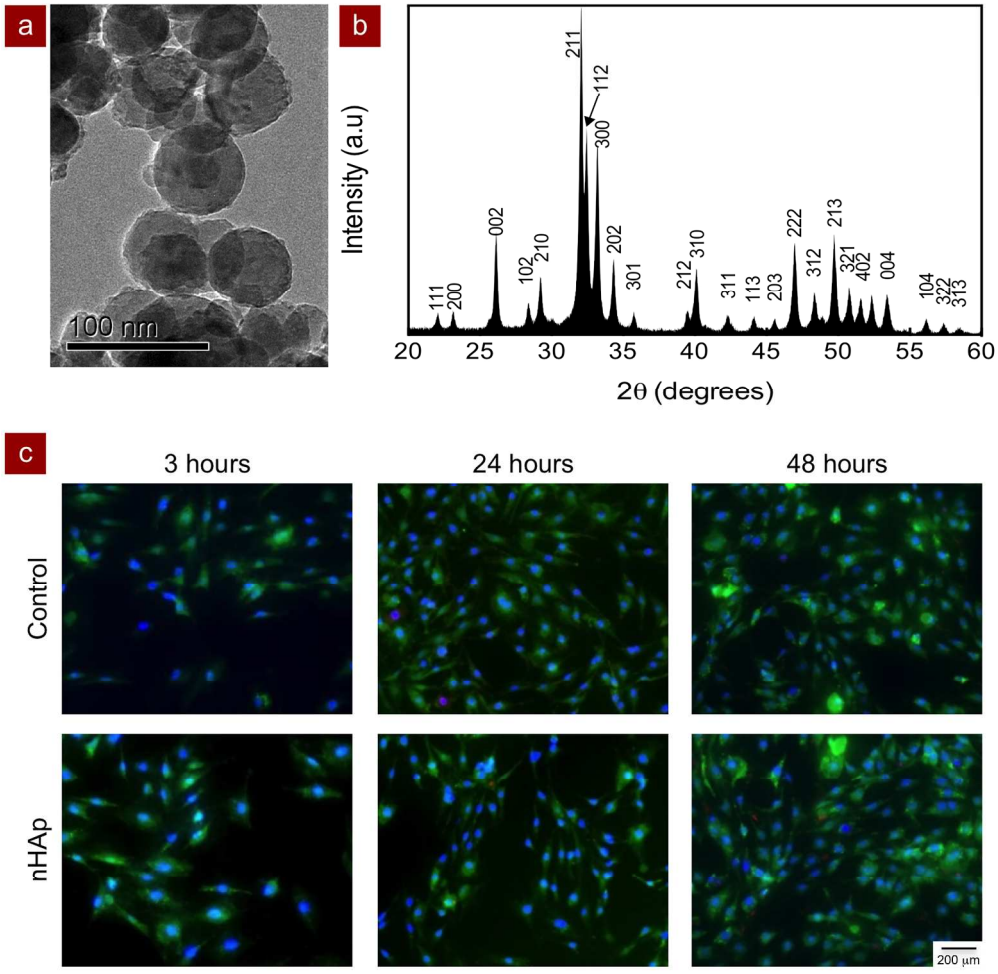

Fig. 1: Structural and in vitro characterization of nHAp. (a) TEM image indicate spherical size of nHAp. (b) XRD data indicates highly crystalline nature of nHAp. (c) In vitro evaluation indicates no significant effect of nHAp on cell viability of proliferation.
254x247mm (300 x 300 DPI)

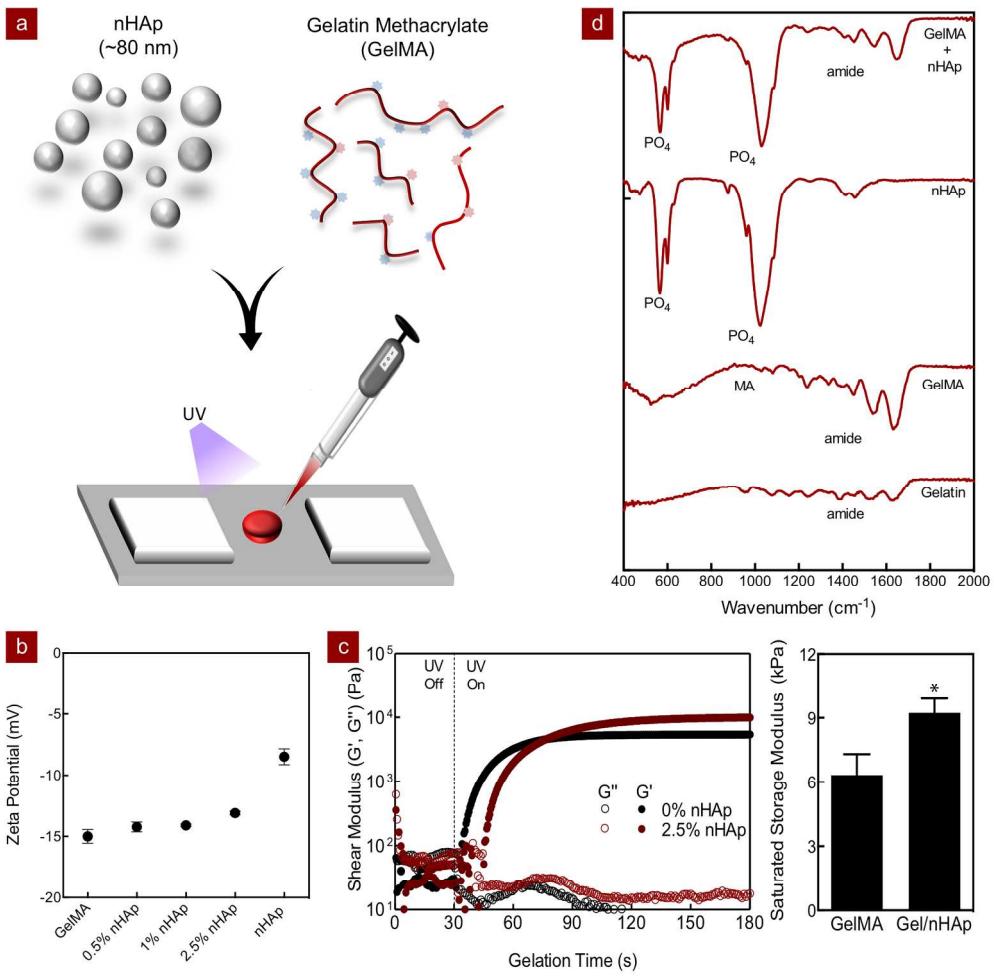

Fig. 2: Synthesis of nanocomposite hydrogels from nHAp and GelMA. (a) nHAp combined with prepolymer solution containing GelMA was subjected to UV to obtain covalently crosslinked hydrogel network. (b) FTIR spectra indicate presence of nHAp within hydrogel network. (c) No significant change in zeta potential was observed due to addition of nHAp indicating limited interactions between nanoparticle and polymer. (d) UV rheology indicates formation of covalently crosslinked network upon UV exposure as observed by the saturation of strorage modulus (G'). The presence of nHAp delays the onset of crosslinking process due to ability of nHAp to observe UV light. (*p<0.05, One-way ANOVA followed by Tukey post-hoc multi-comparison testing).
254x249mm (300 x 300 DPI)

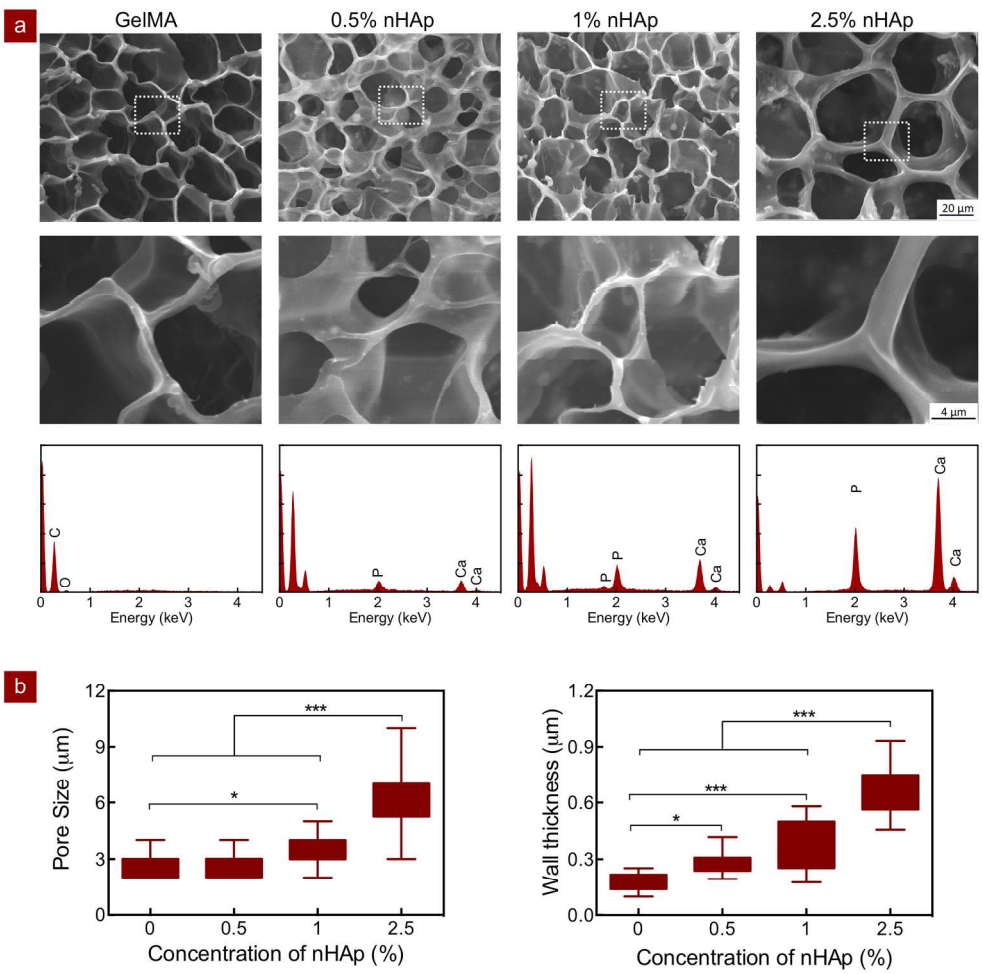

Fig. 3: The effect of nHAp in nanocomposite network. (a) All the hydrogels exhibit porous and interconnected networks. The addition of nHAp results in formation of a hydrogel network with larger pore size. EDS spectra indicate presence of Ca and P in the nanocomposite network. (b) The effect of nHAp addition on pore size and pore wall thickness in the polymer network was quantified using ImageJ. 254x246mm (300 x 300 DPI)

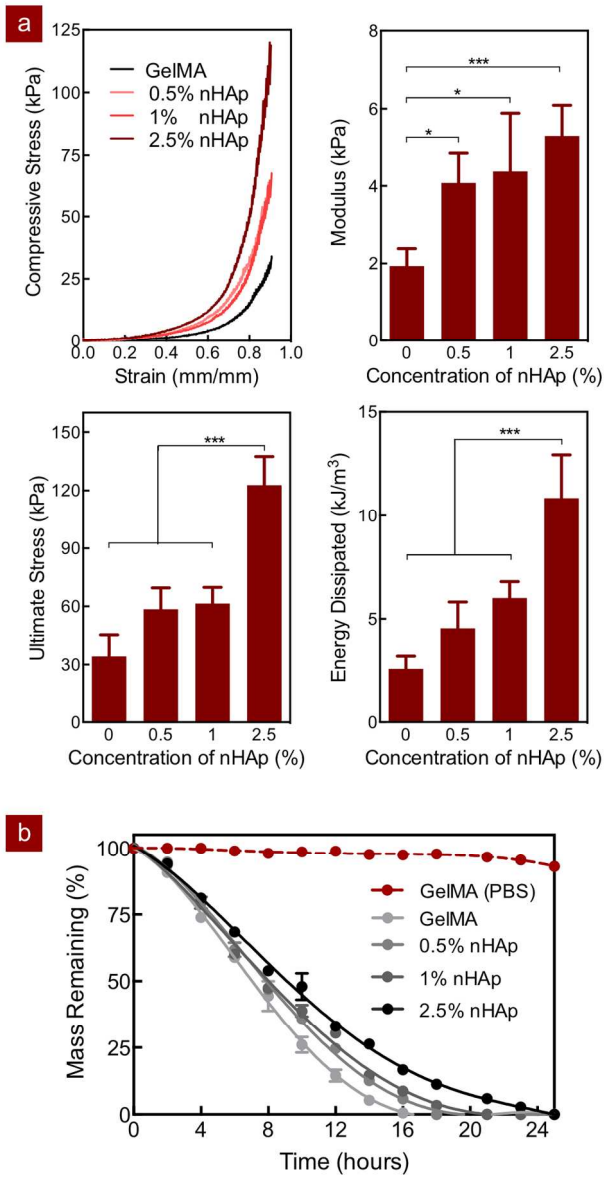

Fig. 4: The effect of nHAp on the mechanical stiffness and physiological stability of nanocomposite hydrogels. (a) The stress-strain curve indicates increase in modulus, ultimate stress and energy dissipated due to addition of nHAp. (b) The degradation rate of nanocomposite hydrogel decreases with the addition of nHAp.
127x247mm (300 x 300 DPI)

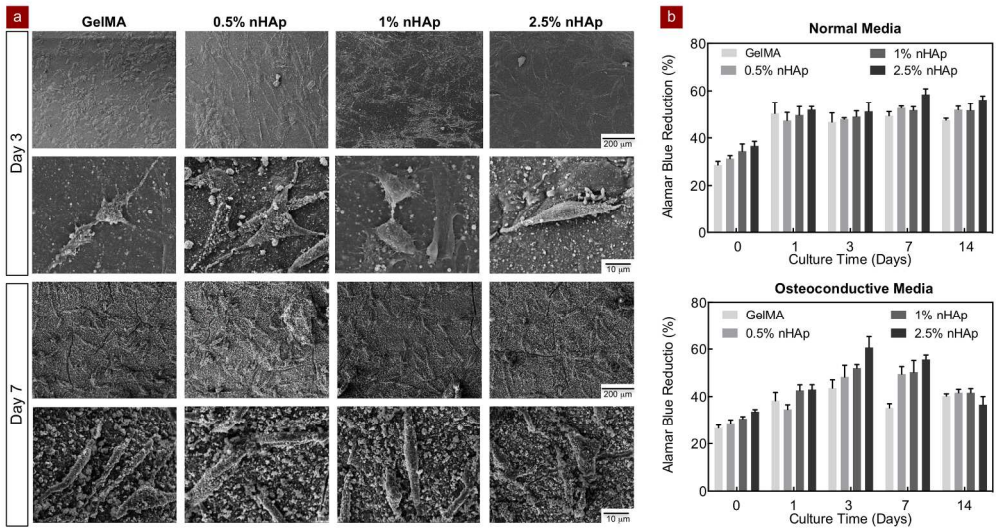

Fig. 5: Cell adhesion, spreading and proliferation on nanocomposite hydrogels. (a) Cells readily adhere and spread on all the nanocomposite samples. (b) The addition of nHAp does not significantly affect cell proliferation.
254x136mm (300 x 300 DPI)

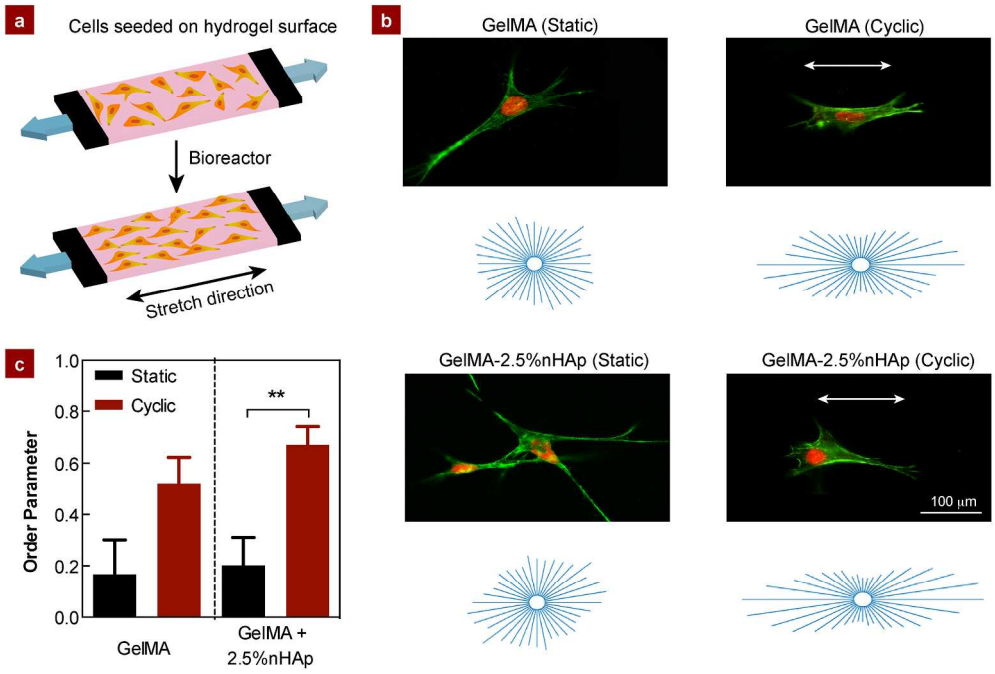

Fig. 6: Cyclic stretching inducing cell and stress fiber (SF) alignment on elastomeric nanocomposite hydrogels. (a) Preosteoblasts are seeded on the hydrogel surface and subjected to cyclic stretching (0.08 strain, 1 Hz, 6 h). (b) Representative images are shown of non-confluent preosteoblasts subjected to static conditions or cyclic stretching when cultured on GelMA and GelMa-2.5%nHAp hydrogels with corresponding SF angular distributions. (c) Order parameters summarizing cell orientation (N=30-50, **p<0.01, One-way ANOVA followed by Tukey post-hoc multi-comparison testing).
254x172mm (300 x 300 DPI)

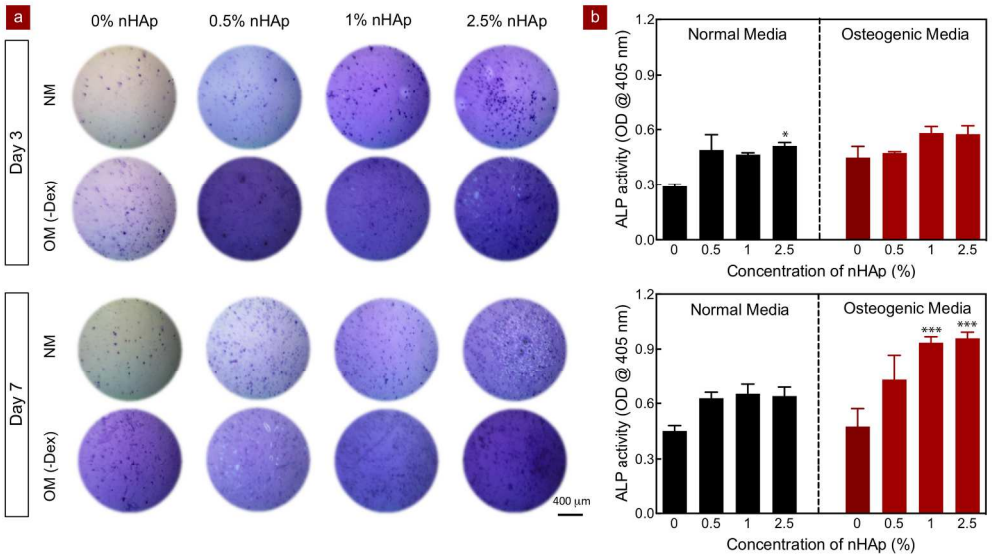

Fig. 7: The effect of nHAp on ALP staining and activity. (a) The addition of nHAp to GelMA significantly enhances ALP staining on Day 3 and Day 7 in normal (NM) and osteoconductive (OM) media. (b) A similar trend is observed in the ALP activity on day 3 and 7 in both normal and osteogenic conditions. (*p<0.05, ***p<0.001, One-way ANOVA followed by Tukey post-hoc multi-comparison testing).
254x142mm (300 x 300 DPI)

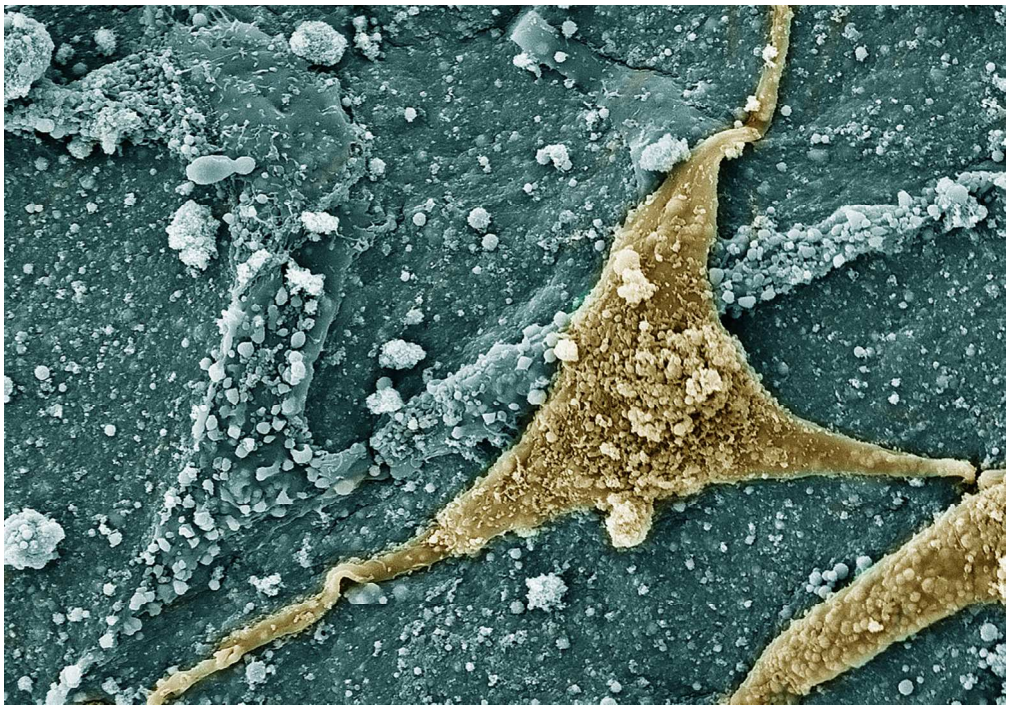

Table of Content: We report synthesis and characterization of photocrosslinkable nanocomposite hydrogels from nanohydroxyapatite (nHAp) and gelatin methacryloyl (GelMA). The addition of nHAp to GelMA increases mechanical stiffness, supports cell proliferation and enhances osteogenic response of seeded preosteoblast.
127x88mm (300 x 300 DPI)